Composite Structures 335 (2024) 117998

Contents lists available at ScienceDirect

Composite Structures

journal homepage: www.elsevier.com/locate/compstruct

A modified equally-spaced method (MEQS) for fibre placement in additive manufacturing of topology-optimised continuous carbon fibre-reinforced polymer composite structures

Shuai Wang [a,b], Haoqi Zhang [a], Aonan Li [a], Junaid Ahmad Abdul Qayyum [a], Yongxing Wang [c], Zhelong He [b], Jie Liu [b,*], Dongmin Yang [a,*]

[a] School of Engineering, Institute for Materials and Processes, University of Edinburgh, EH9 3FB Edinburgh, UK
[b] State Key Laboratory of Advanced Design and Manufacturing for Vehicle Body, College of Mechanical and Vehicle Engineering, Hunan University, 410082 Changsha, China
[c] School of Computing, University of Leeds, LS2 9JT Leeds, UK

ARTICLE INFO

Keywords:
Topology optimisation
Additive manufacturing
Printing path planning
Continuous fibres
Finite element analysis

ABSTRACT

This study proposes a modified equally-spaced (MEQS) method for the path design of continuous fibres in additive manufacturing (AM) of topologically optimised composite structures. The MEQS method addresses the low fibre infill rate issue of the traditional Equally-Spaced (EQS) method by utilising the Offset method to generate looped printing paths around the internal cavities and gaps between continuous fibre paths. The developed MEQS method was first illustrated against EQS and Offset methods using an open-hole composite plate in which topology and material orientation were simultaneously optimised using the discrete–continuous parameterisation (DCP) method. Actual printing path-based finite element modelling showed that the MEQS method achieves a 25.32% increase in stiffness compared to the Offset method. Experimental testing of the additively manufactured open-hole composite plates showed that the MEQS method improves the stiffness and strength by 15.52% and 27.38%, respectively, compared to the Offset method. The proposed MEQS was further demonstrated through two other case studies by finite element modelling, showing that the stiffness of MEQS has increased by an average of 66.71% and 14.95% compared to EQS and Offset, respectively.

1. Introduction

Carbon fibre-reinforced polymer (CFRP) is a widely used composite material in aerospace, automotive, wind energy and sports industries, due to its high stiffness and strength [1]. Notably, CFRP exhibits superior stiffness-to-weight ratio compared to metallic materials like titanium and aluminium alloy, rendering it an appealing choice for lightweight design [2]. The lightweight performance of CFRP composite structures can be further enhanced by topology optimisation to eliminate the materials that have minimal impact on the overall structural response.

Various topology optimisation methods have been developed, including the homogenisation method [3], Solid Isotropic Material Penalization (SIMP) [4,5], Level-set method (LSM) [6,7], Evolution Structural Optimisation (ESO) [8,9], and other feature mapping methods [10–12]. For the traditionally manufactured CFRP laminates with [0/±45/90]s stacking sequences, the above techniques could be adopted directly, as their properties could be considered quasi-isotropic. However, traditional machining processes used for composites with complex geometry after optimisation, such as drilling and cutting, would induce defects of fibre pull-out, fibre breakage and/or delamination, thus deteriorating the mechanical performance of composite structures [13–15]. As an alternative, additive manufacturing (AM) techniques offer the potential to manufacturing CFRP structures with relatively complicated geometries while maintaining fibre integrity. For instance, the material extrusion technique can deposit continuous fibres along designed paths to create geometric singularity [16].

Topology optimisation of general anisotropic composites has been more challenging. Discrete Material Optimisation (DMO) was developed to transform anisotropic topology optimisation problems into multiple anisotropic material selection problems [17]. Continuous Fibre Angle Optimisation (CFAO) was developed based on SIMP, which acquires

* Corresponding authors.
E-mail addresses: liujie@hnu.edu.cn (J. Liu), Dongmin.Yang@ed.ac.uk (D. Yang).

https://doi.org/10.1016/j.compstruct.2024.117998
Received 22 December 2023; Received in revised form 17 February 2024; Accepted 21 February 2024
Available online 24 February 2024

optimal structure by simultaneously optimising density and orientation [18]. Luo *et al.* [19] developed a discrete–continuous parametrisation (DCP) method based on DMO and CFAO. In the DCP method, the searching interval of fibre orientation is divided into several subintervals (2–3 in most cases). The optimal subinterval is first selected, and then the optimal orientation in the subinterval is optimised. All these optimisation methods exported discrete "field information" consisting of a pseudo-density field and a material orientation field. Besides, Elvas *et al.* [20] proposed an optimisation framework to assign material and fibre orientation on discrete patches of the variable stiffness composite laminates. Yan *et al.* [21] concurrently optimised topology and material orientation by transforming the optimisation problem into a multi-scale one. Jantos *et al.* [22] presented a method for simultaneous optimisation of topology and material orientation while controlling the smoothness of the orientation with an efficient filter. However, the above optimisation results cannot be directly used for AM because continuous fibres are printed along continuous paths as much as possible during the AM process.

Over the past few years, several printing path design methods have been developed for continuous fibre filaments. Zhang *et al.* [23] used the principal stress method to design printing paths for topology-optimised composite structures, in which the trajectories of the first and third principal stress are chosen as the printing paths for the continuous fibre filament. Wang *et al.* [24] developed a load-dependent path planning method for AM of CFRP composites. However, intersection issues of the printing paths can barely be avoided by the above method. Papapetrou *et al.* [25] reported two geometry-based methods in their research, *i.e.*, the equally-spaced method (EQS) and the Offset method. For the EQS method, continuous fibre paths are generated parallel to the optimised structure's boundary at equally spaced distances. The paths are controlled by several control points, in which the positions are manually decided. The Offset method generates contour-like fibre paths parallel to the boundary of the structure. Fernandes *et al.* [26] compared EQS and Offset methods through both finite element analysis (FEA) and experiments. In most of their cases, Offset outperformed EQS because of the higher fibre infill rate. However, it should be noted that the fibre infill rate of the EQS method can be increased by modifying design principles, thus achieving the same or even better performance compared to the Offset method. As the EQS method maintains the continuity of fibres in different loading areas, the load could be smoothly transferred, and the stresses could be evenly distributed.

This study presents a fibre path planning method based on geometry for structures that exhibit geometric singularity after topology optimisation. Initially, the DCP optimisation method is employed to acquire an orthotropic material distribution. Subsequently, a modified equally-spaced (MEQS) method is utilised to generate continuous fibre paths. The MEQS method aims to achieve a compact path pattern with a high fibre infill rate while maintaining fibre continuity. To validate the mechanical performance improvement, an experimental investigation was conducted on an unsymmetrically loaded open-hole composite plate. The plate was chosen due to its complex geometry resulting from DCP optimisation, which poses substantial manufacturing challenges. Finite element modelling analysis was performed on different path patterns, including Offset, original EQS, and MEQS, using Texgen [27] and ABAQUS software for comparison. Additionally, experimental studies were conducted on the Offset and MEQS patterns. Samples were 3D printed using continuous carbon fibre-reinforced epoxy filament and consolidated to ensure as-designed fibre paths and low porosity. Stiffness, strength, and failure modes were analysed to evaluate the effectiveness of the proposed method. Furthermore, the mechanism was discussed by analysing stress distribution from numerical modelling. Finally, the proposed MEQS method was demonstrated in two additional numerical case studies.

2. Topology optimisation and path planning method

2.1. Topology optimisation

During the simultaneous optimisation of topology and material orientation, the orientation of each element locates in $[-\frac{\pi}{2},\frac{\pi}{2}]$, in which case the objective function is highly non-convex according to [19]. When the topology and material orientation are optimised simultaneously, it could easily fall into local optima. Thus, the DCP method is used for topology optimisation in this study. The kernel of DCP evenly divides the searching interval of material orientation θ_e into n subintervals ($n = 2$ in this study), determining which subinterval θ_e locates with the help of n discrete variables in the first stage and then searching the optimal θ_e around the midpoints of subintervals. In this way, as long as the subinterval is selected, the searching interval would be much smaller and thus less likely to fall into local optima.

In the DCP method, the optimisation problem can be described as:

$$\begin{aligned} &Minimise: \quad c(\rho,\chi_1,\chi_2,\cdots,\chi_n,\theta) = U^T K(\rho,\chi_1,\chi_2,\cdots,\chi_n,\theta)U \\ &s.t.: \quad \sum_{i=1}^{N}\rho_i \leqslant f_v \times N \\ &\qquad \rho_e \in [\rho_{\min},1] \\ &\qquad \chi_{ie} \in [0,1] \\ &\qquad \sum_{i=1}^{n}\chi_{ie} = 1 \\ &\qquad \theta_e \in [-\frac{\pi}{2n},\frac{\pi}{2n}] \end{aligned} \tag{1}$$

where the compliance c is the objective function of optimisation, ρ is the pseudo-density vector, $\chi_1,\chi_2,\cdots,\chi_n$ are material orientation sub-interval definition parameters, and θ is the local material orientation vector. U is the displacement vector, K is the stiffness matrix, N denotes the total number of elements, and f_v stands for volume fraction. ρ_e stands for element pseudo-density, χ_{ie} is the orientation sub-interval determining parameter (i.e.$\chi_{1e} = 1$ means for element e, the material orientation locates in the sub-interval 1) and θ_e is the element local material orientation, n is the total number of sub-intervals. A lower bound of pseudo-density $\rho_{\min}$ is imposed to avoid the singularity problem.

The stiffness matrix of the structure $K(\rho,\chi_1,\chi_2,\cdots,\chi_n,\theta)$ is assembled as follows:

$$K(\rho,\chi_1,\chi_2,\cdots,\chi_n,\theta) = \sum_{e=1}^{N}(\rho_e)^p K_e(\chi_{1e},\chi_{2e},\cdots,\chi_{ne},\theta_e) \tag{2}$$

where the penalisation parameter p has the same effect as its counterpart does in SIMP, which is intended to punish the pseudo-density between $\rho_{\min}$ and 1. $K_e(\chi_{1e},\chi_{2e},\cdots,\chi_{ne},\theta_e)$ is the anisotropic stiffness matrix of e^{th} element.

According to [18], the element stiffness matrix $K_e(\chi_{1e},\chi_{2e},\cdots,\chi_{ne},\theta_e)$ is obtained by integrations with the help of Gauss quadrature:

$$\begin{aligned} K_e(\chi_{1e},\chi_{2e},\cdots,\chi_{ne},\theta_e) &= \iiint B^T C'(\chi_{1e},\chi_{2e},\cdots,\chi_{ne},\theta_e)B d\Omega \\ &\approx \sum_{i=1}^{n_{gp}}\sum_{j=1}^{n_{gp}}\sum_{k=1}^{n_{gp}}\left(W_i W_j W_k B^T C'(\chi_{1e},\chi_{2e},\cdots,\chi_{ne},\theta_e)B|J|\right) \end{aligned} \tag{3}$$

where n_{gp} is the number of Gauss points, B is the strain–displacement matrix, J is the Jacobian matrix, and C' is the rotated constitutive tensor of the anisotropic material which is defined as:

$$C'(\chi_{1e},\chi_{2e},\cdots,\chi_{ne},\theta_e) = T^T(\theta_e)\cdot C^n(\chi_{1e},\chi_{2e},\cdots,\chi_{ne})\cdot T(\theta_e) \tag{4}$$

in which $T(\theta_e)$ is the transform matrix

$$T(\theta_e) = \begin{bmatrix} \cos^2\theta_e & \sin^2\theta_e & 0.5\cdot\sin 2\theta_e \\ \sin^2\theta_e & \cos^2\theta_e & -0.5\cdot\sin 2\theta_e \\ -\sin 2\theta_e & \sin 2\theta_e & \cos 2\theta_e \end{bmatrix} \tag{5}$$

and $C^n(\chi_{1e},\chi_{2e},\cdots,\chi_{ne})$ is the constitutive tensor after the orientation sub-interval selection process. The selection can be described as (for simplicity of expression, $\chi_{1e},\chi_{2e},\cdots,\chi_{ne}$ are written as χ):

$$C^n(\chi) = W_1(w(\chi))C_1 + W_2(w(\chi))C_2 + \cdots W_n(w(\chi))C_n \tag{6}$$

In function (6), $C_1, C_2, \cdots C_n$ are the constitutive tensors corresponding to the midpoint of the sub-intervals, $W_1, W_2, \cdots W_n$ are weight functions which can be described as:

$$\begin{aligned} W_i &= \frac{w_i(\chi)}{\sum_{j=1}^{n} w_n(\chi)} \\ w_i(\chi) &= \chi_i^q \prod_{j=1}^{n} (1-\chi_{j\neq i}^q) \end{aligned} \tag{7}$$

in which χ_i is a continuous varying design parameter in the interval [0,1], the penalty factor q aims to yield a discrete 0/1 result. It is worth noting that for the purpose of convergence, q is increased from 1 to 3 gradually.

The corresponding orientation angles for $C_1, C_2, \cdots C_n$ are $\theta_1,\theta_2,\cdots,\theta_n$:

$$\theta_i = \frac{(2i-1-n)\pi}{2n} i = 1,2,\cdots,n \tag{8}$$

then $C_1, C_2, \cdots C_n$ can be computed by:

$$C_i = T^T(\theta_i)C_0T(\theta_i) i = 1,2,\cdots,n \tag{9}$$

where C_0 is the unrotated constitutive tensor of orthotropic material which can be expressed as:

$$C_0 = \begin{bmatrix} C_{11} & C_{12} & 0 \\ C_{21} & C_{22} & 0 \\ 0 & 0 & C_{66} \end{bmatrix} \tag{10}$$

The components C_{11}, C_{12}, C_{22} and C_{66} of a 2D orthotropic composite material can be computed from its elastic properties which in turn are calculated from the properties of its fibre and polymer matrix as follows [28]:

$$\begin{cases} C_{11} = E_1/(1-\nu_{12}\nu_{21}) \\ C_{12} = \nu_{21}E_1/(1-\nu_{12}\nu_{21}) \\ C_{22} = E_2/(1-\nu_{12}\nu_{21}) \\ C_{66} = G_{12} \end{cases} \tag{11}$$

$$\begin{cases} E_1 = fE_f + (1-f)E_m \\ E_2 = \left(f/E_f + (1-f)/E_m\right)^{-1} \\ G_{12} = \left(f/G_f + (1-f)/G_m\right)^{-1} \\ \nu_{12} = f\nu_f + (1-f)\nu_m \\ \nu_{21} = \left(f\nu_f + (1-f)\nu_m\right)\dfrac{E_2}{E_1} \end{cases} \tag{12}$$

where E, G, ν represent Young's modulus, shear modulus and Poisson's ratio respectively, the subscripts m and f stand for matrix and fibre, and f is the fibre volume fraction.

2.2. Fibre path planning method

In this section, an open-hole composite plate with unsymmetrical tensile loading is used to illustrate the existing Offset and EQS methods as well as the strategy for the MEQS method. Specifically, a short description of the EQS and Offset workflows is given for a better understanding of the characteristics of EQS and Offset. The principles of the proposed MEQS method and the corresponding printing path pattern are then illustrated.

2.2.1. Open-hole composite plate under unsymmetrical tensile loading

In Fig. 1, the boundary conditions and optimised design of a plate with an open hole are illustrated. To reduce computational costs, only half of the plate is modelled using symmetry. As shown in Fig. 1(a), the model comprises 50 × 100 four-node square elements. A hole with a radius of 15 is located at the centre. Meanwhile, a small ring area outside the hole is set as an off-design area, which means that the material in this area will be excluded from the optimisation to maintain the geometric shape of the hole. As illustrated in Fig. 1(b), the topology and material orientation are simultaneously optimised by the DCP method. In the design area, material that does not contribute much to the mechanical performance is removed. Thus, multiple voids are formed. It is worth noting that all the printing path planning methods involved in this study will first be analysed using the structure in Fig. 1(b) because of its relatively complex geometry, which could better reflect the advantages and disadvantages of each method.

2.2.2. Current printing path planning methods – Offset and EQS

The EQS method generates the fibre paths that are equally placed in the optimised structure. It organises paths defined by a set of control points along the main dimension of the structure (y-axis in the current case). The EQS method slices the structure along the direction transverse to the main dimension at multiple key positions, which is called the slicing procedure in this study. The key positions are where the structure is divided into several branches, or the branches are merged, as Fig. 2(a) shows. Then, control points are arranged equally in every branch of the slices; it is worth noting that the total number of control points for every slice is constant, while the number of control points in every branch can be decided manually. The process starts at the simplest geometry of the structure (downside for the given case) for the convenience of organising the distribution of control points. Finally, the control points are connected by splines along the main direction. As Fig. 2(a) shows, all the printed continuous carbon fibre filaments are arranged in black, and the fibre paths are highly smooth along the main direction, which facilitates

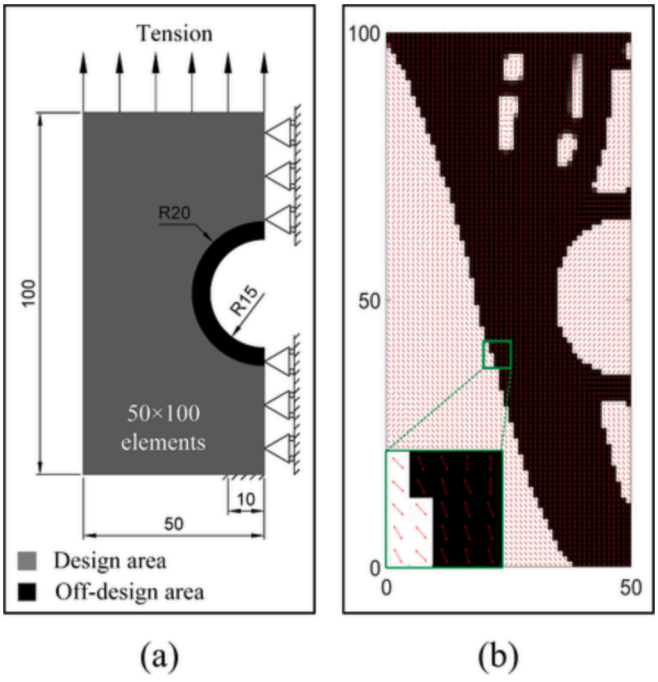

Fig. 1. (a) Boundary conditions of the open-hole case and (b) DCP optimisation result.

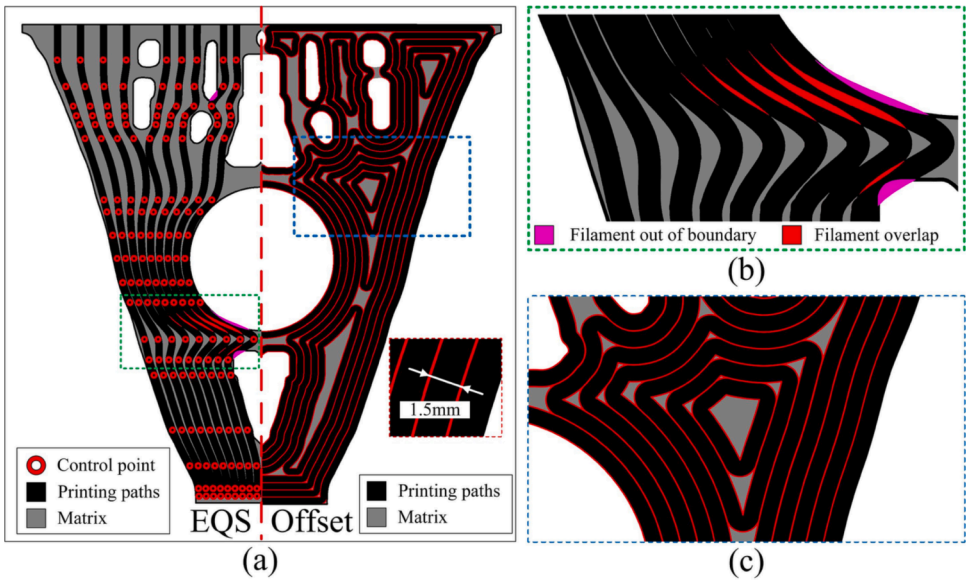

Fig. 2. (a) Printing paths designed by EQS and Offset methods, (b) Out-of-boundary and overlap issues, (c) Loop-like pattern.

AM since there are very few sharp corners in the paths. However, the structure has some relatively large area without embedded filaments, negatively affecting the mechanical behaviour.

Moreover, the control points for the paths are placed artificially; meanwhile, a slight change of the control points' coordinates affects the paths to a great extent. As illustrated in Fig. 2(b), two undesirable phenomena will occur when the control points are placed in the wrong position: filament overlaps and out-of-boundary filaments. The first phenomenon will cause the manufacturing issue of fibre stacking. More importantly, the second phenomenon results in discrepancies between the 3D printed part and the initial topology optimisation design.

The Offset method creates fibre paths which are parallel to the structure boundary, as shown in Fig. 2(a). The first set of paths are generated around the voids, and the next set of paths are created at a given distance equal to the filament width. The procedure continues until the newly generated paths just start to intersect the previous ones. Compared with EQS, the Offset method guarantees a more compact path layout, leading to a higher fibre infill rate. However, flaws still exist in this method. As illustrated in Fig. 2(c), while infilling the structure compactly, fibre paths with undesirable sharp corners will occur, which causes misalignment or even breakage of fibres while printing and thus impairs the mechanical behaviour. Additionally, the loop-like path pattern shown in Fig. 2(c) is difficult to print without modifying the continuous loops, which inevitably introduces artificial factors into the printing path design procedure, as the location of the breakpoints of the existing loops must be specified by the designer. Moreover, in certain scenarios, loop-shaped printing paths may not efficiently bear the load. As depicted in Fig. 2(c), the printed fibre filaments are perpendicular to the tensile direction instead of being distributed along it. This observation suggests that the Offset method does not effectively utilise the space within the structure.

2.2.3. *Modified equally spaced method (MEQS)*

Based on the descriptions above, a modified version of EQS is presented, which utilises the advantages of both EQS and Offset. The procedure of MEQS will be introduced using the above case for better

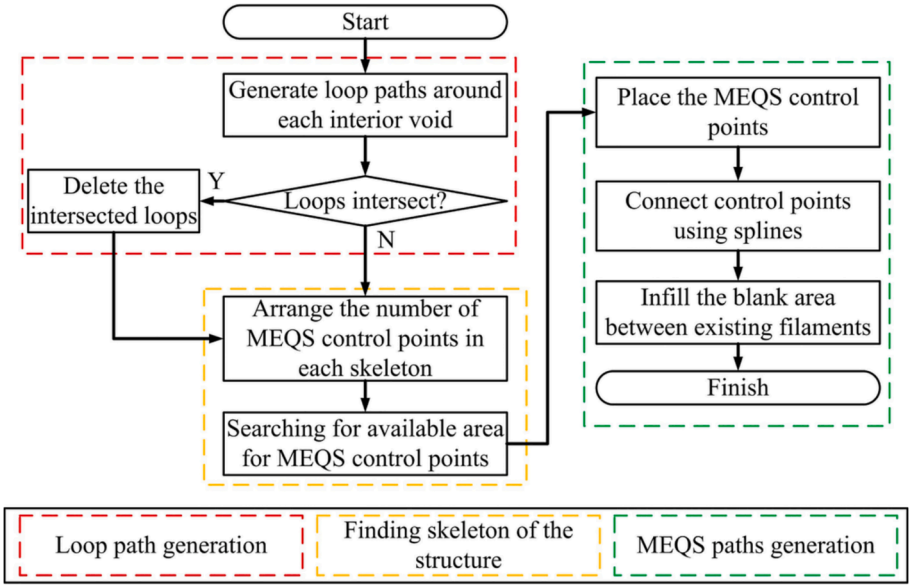

Fig. 3. Flowchart of the MEQS method.

comparisons. Fig. 3 illustrates the workflow of the MEQS method. It can be seen that the MEQS method involves three steps: Loop path generation, finding the skeleton of the structure and MEQS path generation.

The procedure of MEQS path generation is given in Fig. 4. For the convenience of display, only the left half of the structure is demonstrated. In [25], researchers concluded that stiff structures rely both on continuous load paths and reinforcement of the inner voids. Thus, in the first step, an Offset-like procedure is used to generate loop paths and strengthen the edges of the interior voids (illustrated in Fig. 4(a1) and (a2)). Unlike Offset, the looping procedure is only performed once at this stage. Filaments which boundaries interacting with others are deleted to prevent the merging of looped paths. This approach strengthens the edges of the interior voids and allows enough space along the main direction of the structure for the subsequent dense arrangement of fibre filaments.

The second step is to arrange the distribution of the MEQS control points. As previously mentioned, in the EQS method, the position of control points significantly affects the arrangement of printing paths, influencing the mechanical performance of the printed part. Therefore, to address this issue, the MEQS method introduces a principle for slicing to avoid placing control points in the wrong positions. To achieve this, the structure's skeleton is identified with the help of the algorithm presented in [29], as shown in Fig. 4(b1). Black pixels distributed in the direction orthogonal to the main direction (y-axis in this case) are deleted. Finally, the spur and isolated pixels are removed using the 'bwmorh' function in Matlab. The rest of the skeleton graph is illustrated in Fig. 4(b2), which reveals a rough outline of the original sophisticated structure and instructs the distribution of MEQS control points. When the slicing procedure is conducted, the slice may intersect with the structure boundary and skeleton. In one single slice, the intersection points with the boundary are named as $PB_1, PB_2, \cdots, PB_n$, and the ones with the skeleton are named as $PS_1, PS_2, \cdots, PS_m$, n and m denote the time of intersection with the boundary and skeleton separately. The slicing principle is given in Eq. (11). Once satisfied, the slice is defined as an effective slice, meaning the MEQS control points can be placed on the prescribed slice.

$$\begin{cases} n = 2m \\ \dfrac{\max(\|PS_i - PB_{2i-1}\|, \|PS_i - PB_{2i}\|)}{\min(\|PS_i - PB_{2i-1}\|, \|PS_i - PB_{2i}\|)} \leqslant 2 \end{cases} \quad i = 1, \cdots, n \tag{11}$$

In Eq. (11), $\|\cdot\|$ denotes the Euclidian distance between two points. An example of slicing is given in Fig. 5. After several slicing operations and using Eq. (11) to determine the effectiveness of the slices, the results shown in Fig. 4(b3) can be obtained, in which the green area represents the regions where MEQS control points can be placed. In contrast, the red area is the opposite.

After identifying the feasible area for placing MEQS control points, the feasible area is sliced for another time and perpendiculars between the midpoint of the slice and boundaries (or loop paths) are generated, then MEQS control points are distributed along the perpendiculars in which distances between the points equal to the width of filaments, as shown in Fig. 4(c1) and (c2). The locations where branches appear in the structure will also lead to the formation of branches in MEQS paths. The number of MEQS control points in each structural branch is directly proportional to the branch width, which can be roughly estimated using the method described in Eq. (11). It is also worth noting that if the slice line intersects with the skeleton for one time, the MEQS control points are distributed along both two boundaries beside the skeleton. In other

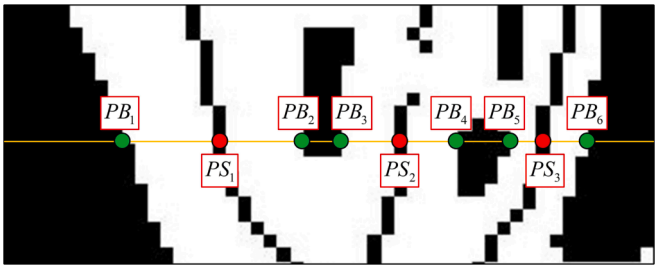

Fig. 5. Slicing procedure of the MEQS method.

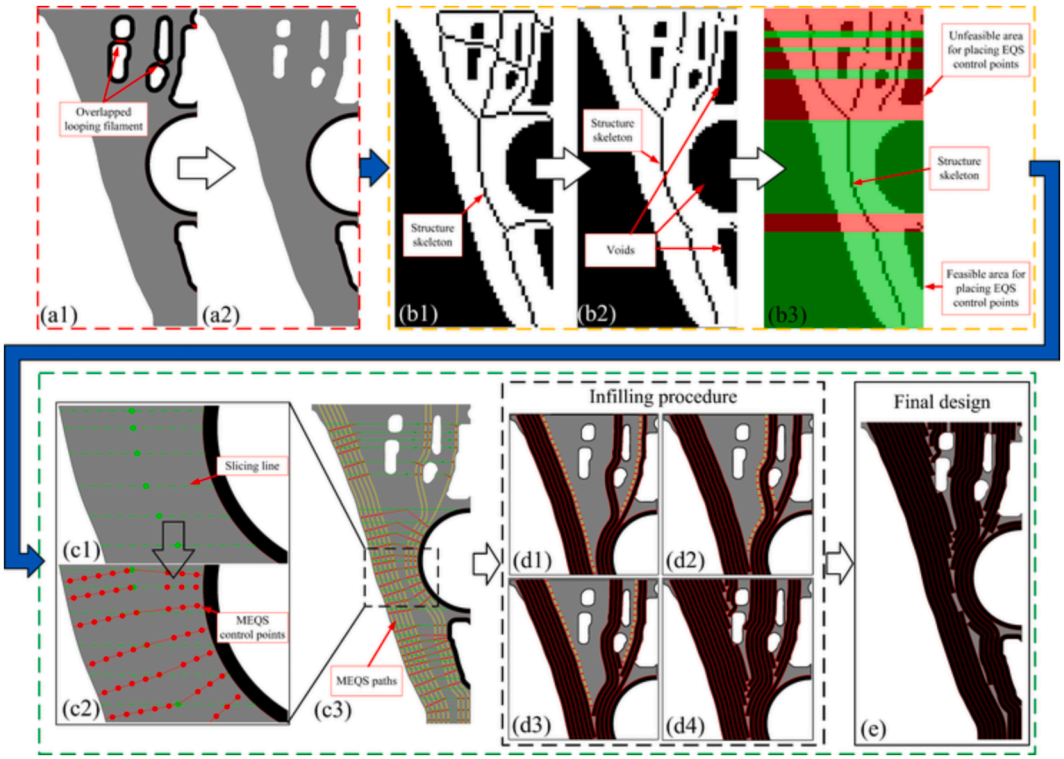

Fig. 4. Procedure of the MEQS path generation.

circumstances, if the slice line intersects with the skeleton multiple times, the MEQS control points would be arranged along only one boundary beside the skeleton which minimises the curvature of the filament. Once the control points are placed, the MEQS paths are generated by connecting points with splines. In some circumstances, where the splines are not able to reach the boundary of the structure, the splines will be extended along the directions defined by the last two control points of the splines until the paths reach the structure boundaries. The MEQS paths generated in this step are illustrated in Fig. 4(c3).

The final step of MEQS path generation is to fill the gaps between all existing MEQS filaments and voids. Fig. 4(d1) - (d4) illustrates the detailed process of the filling procedure. The spaces without filaments are defined as filling spaces and are then sliced following the procedure in the last step. Each time the space is sliced, the distance between adjacent filaments is estimated, a start point of filling filament is set once the space is ample enough to contain a filament, and then control points of filling filaments are distributed along one of the boundaries of the space until the control point reaches the boundary of the filling space. After that, the next round of control point placement will proceed along the other boundary of the space to be filled. After several rounds of alternating filling, the space is fully filled with MEQS paths, marking the end of the MEQS path design process. The printing path designed by the MEQS method is shown in Fig. 4(e). Evidently, the phenomena of filament overlapping and filament out of boundary are eliminated.

3. Finite element modelling and experimental validation

3.1. Finite element modelling

3.1.1. Path-based finite element modelling

To investigate the mechanical behaviour of the proposed MEQS method, finite element analysis (FEA) of all mentioned path planning methods for the above case are performed after 3D printing path generation. It should be noted that in structures with the same geometric profile, the fibre volume fraction plays a crucial role in the mechanical performance of the structure. Therefore, to ensure the rigor of this study, in the design of printing paths using the three different methods mentioned above, efforts were made to maximise the fibre volume fraction.

Following the approach developed in our previous work [23], the finite element models based on the actual printing paths of the continuous fibre filament are built using TexGen software by transforming the printing paths into voxel meshes. Python files coded with the coordinates of the printing paths are imported into Texgen to create printed continuous fibre filament meshed with C3D8R elements. Meanwhile, the material orientation of each element is also automatically defined by Texgen. The meshes are imported into finite element software ABAQUS and embedded into the epoxy matrix model for analysis. T300 carbon fibre and PE6405 Epoxy are adopted as fibre reinforcement and matrix in the continuous fibre filament. The gaps between the adjacent printing paths/filaments are filled with epoxy. Detailed elastic properties are listed in Table 1.

It is worth noting that due to the difficulty of applying the tensile load on the structure boundaries during the mechanical tests, the top and bottom ends of the topology-optimised structures are extended to accommodate the clamps, while the same approach has been taken in [30] and [31]. As shown in Fig. 6, the area for the clamps is given in yellow, and the length of the clamp area is 30 mm. Additionally, the embedded voxel meshes for the printed continuous fibre filaments are illustrated in Fig. 6. The clamp areas are set as rigid bodies in ABAQUS. A load is applied on the lower clamp area along the direction of the red arrow in Fig. 6, whilst the clamp area on the top is fixed.

Table 1
The elastic properties of the materials used in the finite element model.

	E_1 (GPa)	E_2 (GPa)	G (GPa)	v12	v21
Continuous carbon fibre/epoxy filament	84.481	6.105	2.231	0.339	0.025
PE6405 Epoxy	3			0.370	

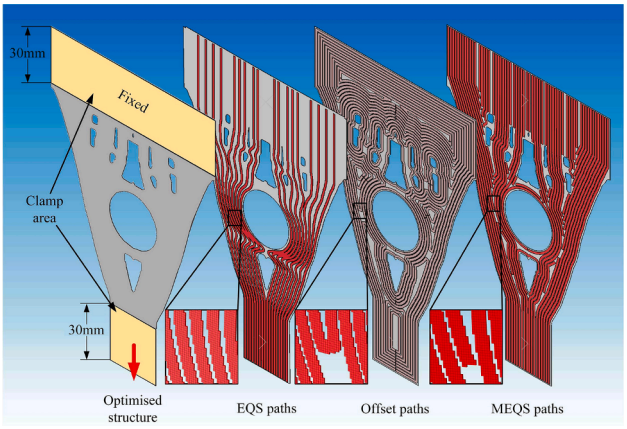

Fig. 6. The optimised structure with embedded voxel meshes of printed continuous fibre filaments/paths.

3.1.2. Mechanical response of the models

The mechanical behaviours of the three models are given in Fig. 7. In this study, the reciprocal of the structural elastic strain energy is used as a measure of structural stiffness. The stiffness of EQS, Offset and MEQS models are $8.439 \times 10^{-5} J^{-1}$, $10.885 \times 10^{-5} J^{-1}$ and $13.641 \times 10^{-5} J^{-1}$, respectively. The performance of the printing paths generated by the EQS method is relatively worse, possibly due to its low filling rate. The MEQS method performs the best, with a mechanical performance improvement of 60.62 % compared to the EQS method, while the Offset method improves 28.17 % over the EQS method.

The principal stress distribution of different models under the load is also illustrated in Fig. 7. It can be seen that the maximum principal stress is mainly concentrated in the continuous fibre filaments on the outer side of the structure. Compared to the printing paths designed by the EQS and Offset methods, the MEQS printing path shows more uniform load transfer, resulting in a relatively less stress concentration. Furthermore, by observing the distribution of the minimum principal stress, it can be seen that the loop-like printing path generated by the MEQS method around the central hole of the structure contributed to bearing the compressive stress, which is consistent with the original

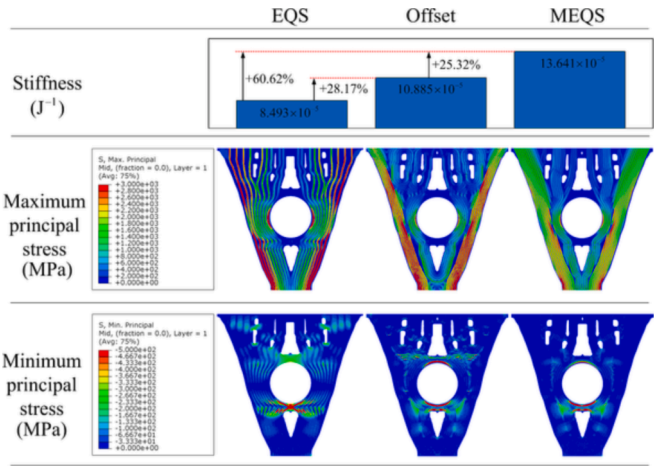

Fig. 7. Stiffness comparison and principal stress distribution in different models.

design intention.

Since none of these three methods can achieve a 100 % fibre infill rate, fibres are unevenly distributed in the structure, and stress concentration may occur in the resin-rich areas. The level of stress concentration can to some extent indicate the possibility of matrix material failure. From Fig. 8, it can be seen that the von Mises stress concentration in the EQS printing path is quite large, located around the central hole of the structure. On the contrary, due to the relatively higher fill rate of the Offset and MEQS method, fewer resin-rich areas exist in the structure. Thus, severe stress concentration is avoided.

3.2. Manufacturing and mechanical testing

3.2.1. As-designed manufacturing

Due to the relatively large gaps between printed continuous fibre filaments in the EQS model, it is challenging to fill up the gaps using epoxy and manufacture good-quality samples without large voids for the mechanical test. The above FEA has already confirmed the lower stiffness and more significant stress concentration of the EQS paths as compared to the MEQS. Therefore the experiments are focused on the comparison between MEQS and Offset methods. For ease of manufacturing, printing paths generated by Offset and MEQS were slightly adjusted before printing. As depicted in [26], the Offset printing path comprises multiple close loops that cannot be practically printed without executing a cutter. Thus, the loops were connected with the adjacent ones. The modified Offset printing paths are given in Fig. 9. Clearly, the printing paths were adjusted to become continuous paths.

On the other hand, discontinuous paths generated in the final step of the MEQS method were also hard to print. So the paths were connected in the same way while keeping the longest possible paths. Some printing paths that extend beyond the boundaries of the structure were generated (highlighted in red in Fig. 9) while modifying the printing paths. These extra sections were trimmed off after the printing. It should be noted that the post-processing for the print paths will to some extent alter the distribution of the original print path, inevitably affecting the mechanical performance of the structure. However, on the other hand, this post-processing procedure will ensure the manufacturability of the structure, which means that 3D printing can be achieved without using a cutter to cut the filament at the edges.

As the printing paths were modified to continuous ones, a Prusa i3 MK3s without a filament cutting mechanism was used for printing the continuous fibre filament. The commercial Markforged nozzle with a diameter of 1.3 mm was used, the nozzle temperature was set as 120 °C, the printing bed temperature was 20 °C, and the printing speed was 15 mm/min. The thickness of one layer of the printed fibre filament was 0.15 mm, and the final printed composite preform consisted of 10 layers of material in total. The 3D printer setting is illustrated on the left side of Fig. 10.

To fill the gaps between the printed continuous fibre filaments, a post-processing method similar to the previous study [32] was adopted in this research. The post-processing of the samples is shown on the right side of Fig. 10. A sufficient amount of epoxy powder was sprinkled between the sheets to fill the gap in the printed preform, which was sandwiched by two thin PLA sheets (with a thickness of 0.4 mm) which acted as a mould for maintaining the position of the printed continuous

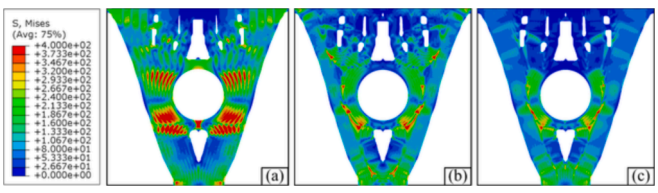

Fig. 8. Von Mises stress distribution in different models: (a) EQS, (b) Offset and (c) MEQS.

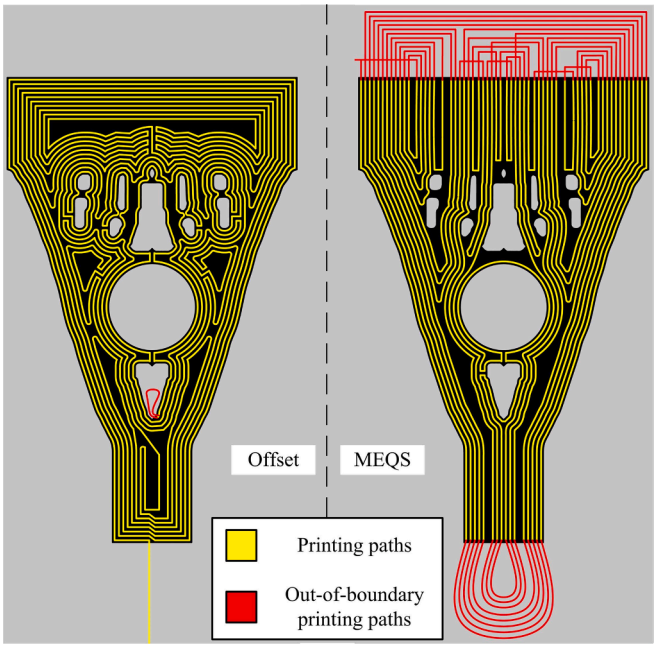

Fig. 9. Modified printing paths after considering manufacturability.

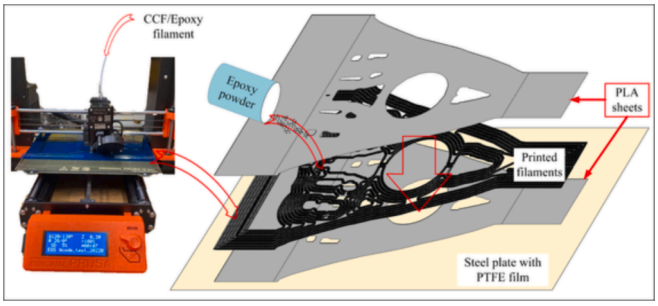

Fig. 10. 3D printing and curing processes of the samples.

fibre filaments during the subsequent curing process. Finally, the assembly was placed in a vacuum bag and cured in an oven. The curing procedure was started by raising the temperature to 40 °C and maintaining for 8 h to remove moisture from the epoxy powder. Then, the temperature was raised to 120 °C and held for 2 h. At this temperature, the powder was fully melted and infiltrated the voids between the fibres. Finally, the temperature was raised to 180 °C and maintained for 2 h to fully consolidate the composite structure.

3.2.2. Mechanical testing

The experimental set-up of the tensile test is given in Fig. 11. The tests were conducted using an Instron 8802 testing machine, which was equipped with 100 mm wide clamps to fully grab the test samples. The upper clamp of the 8802 testing machine was fixed while the lower clamps were loaded downward at a speed of 0.5 mm/min. Speckle patterns were applied to the surfaces of the samples for the 2D digital image correlation (DIC) measurement of the planar strains. The data collected from the high-speed camera was processed using Ncorr [33], which has also been used in previous studies [23,32].

3.2.3. Mechanical performance

A set of load–displacement curves is plotted in Fig. 12(a); the stiffness of the Offset sample and MEQS stiffness are 17.45 kN/mm and 20.16 kN/mm, respectively. The failure happened when the load reached 11.57 kN and 14.00 kN. The statistical data of all the printed

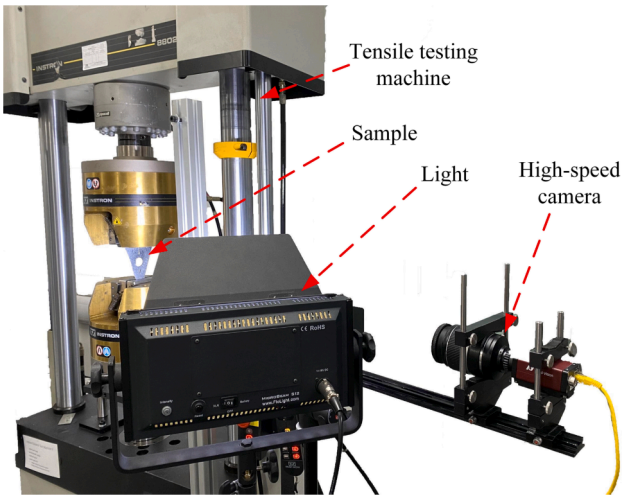

Fig. 11. Experimental set-up of the tensile test of the topology-optimised structure.

samples is illustrated in Fig. 12(b). It can be concluded that, for this specific case, the MEQS path exhibits a certain degree of improvement in both stiffness and strength, i.e. the stiffness was increased by an average of 15.52 %, while the strength was increased by an average of 27.38 %.

For the sample based on the Offset printing path, when the load reached 11.18 kN, there were clear cracks in the sample, which is shown in Fig. 13(a). The cracks propagated as the loading continued until it reached 11.57 kN for failure. The final distribution of the cracks is shown in Fig. 13(b), in which the yellow lines represent the propagated cracks. A noticeable fibre fracture occurred in the upper left part of the sample. By comparing the crack distribution in Fig. 14(b) with the Offset printing paths, it can be observed that the orientation of the cracks was generally consistent with the direction of the printing path, as illustrated in Fig. 13(c). The possible reason for this phenomenon is that the matrix material between the fibre filaments first experienced failure under localised tensile and shearing stresses. Then, the cracks rapidly propagated along the typical loop-like structure of the Offset printing path. Within a short period after the first appearance of the cracks, there was a distinct redistribution of stresses in the sample, eventually leading to stress concentration in the upper left region of the sample and causing the failure.

A similar phenomenon was also seen in [30], in which a three-point-bending beam was first optimised and 3D printing path was then generated according to the structure's geometry. In [30], the optimised structure was infilled by loop-like paths. However, certain parts of the structure were subjected to tensile stress. During the loading process, the matrix between the fibre filaments in these areas experiences damage under the tensile stress, leading to matrix cracking. Ultimately, the fibres in the sample break due to stress redistribution and crack propagation, resulting in the failure of the sample.

For the sample based on the MEQS printing path, the cracks first appeared at the bottom of the sample when the load reached 8.94 kN, as given in Fig. 14(a). In the MEQS sample, there are relatively fewer printing paths of continuous fibre filament around the interior voids,

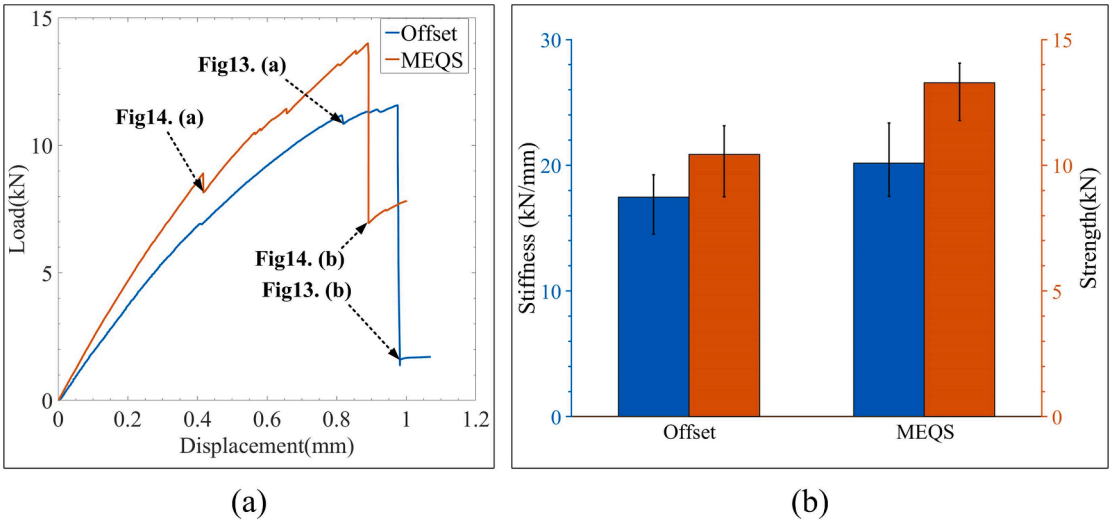

Fig. 12. (a) Load-displacement curves and (b) stiffness and strength results of Offset and MEQS path-based samples.

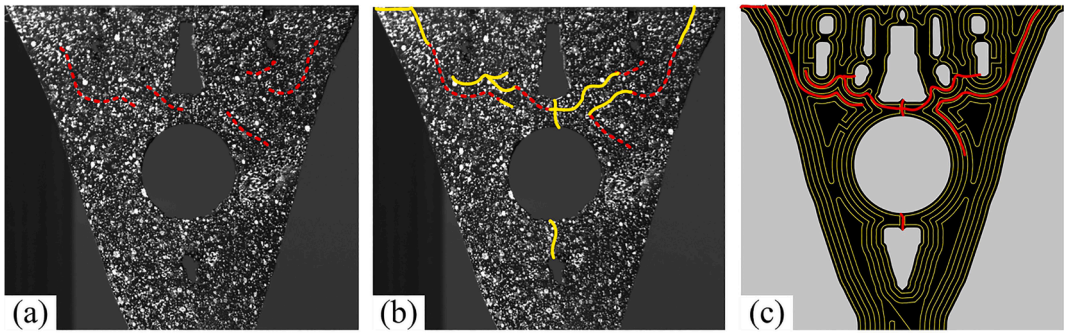

Fig. 13. Propagation of cracks in the Offset sample: (a) initiation of small cracks, (b) crack coalesce to cause the failure, and (c) locations of the cracks against the designed printing paths.

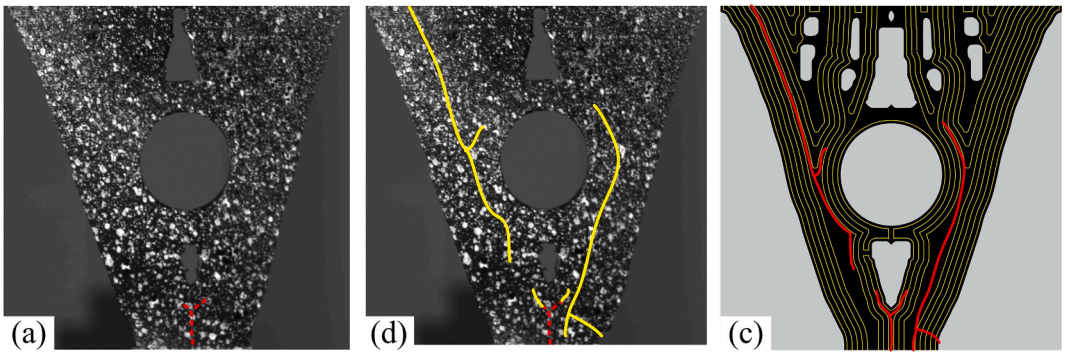

Fig. 14. The distribution of cracks in the MEQS samples at different stages: (a) before the crack propaagtion, (b) before the failure of the Offset sample, and (c) the relative position of the cracks and the printing paths.

which means that the matrix lacks reinforcement from the fibres compared to the Offset paths. Thus, the matrix suffered an early failure in the bottom area. However, it must be noted that the crack did not split the sample in half but rather ceased further upward expansion and extended sideways at a certain location, ultimately forming a Y-shaped crack (illustrated by the red dashed lines in Fig. 14(a)), which can be attributed to the loop-like path around the void. This phenomenon confirms the effectiveness of the MEQS trajectory design method by placing fibres around the interior voids to reinforce them while preserving as many continuous fibres as possible to facilitate the transmission of forces between the loading boundary and the fixed boundary. As the load continued, more cracks were generated on both sides of the central hole. When the load reached 14.00 kN, the fibres in the lower right part of the sample failed, resulting in the splitting and failure of the sample. The distribution of the cracks is given in Fig. 14(b), in which the yellow lines represent the propagated cracks. Same as before, the cracks were correlated with the printing paths of continuous fibre filament in Fig. 14 (c). It can be seen that, due to the absence of the abundant loop-like structure in the MEQS paths, there was no extensive transverse matrix damage in the sample when the failure occurred.

Furthermore, the strain on the horizontal and vertical direction acquired by DIC and FEA are given in Fig. 15 and Fig. 16, respectively. In the two figures, six regions that reflect the similarities between the DIC data and the FEA results are highlighted. In Region 1 and 2, it can be seen that the matrix and fibre below the central hole suffered compression in the horizontal direction. By observing Region 3 in Figs. 15 and 16, it can be seen that both DIC data and FEA results showed significant deformation in the vertical direction in this region. Comparing with the Offset printing path shown in Fig. 9, the significant deformation occurred exactly in the areas where the loop-like printing path is located. The looped fibres failed to bear the applied tension in the vertical direction, resulting in pronounced deformation. In Regions 4 to 6, the DIC data and FEA results are generally consistent. In these regions, the printed paths of continuous fibre filament exhibit bending, which may be the reason for the noticeable deformation at this location.

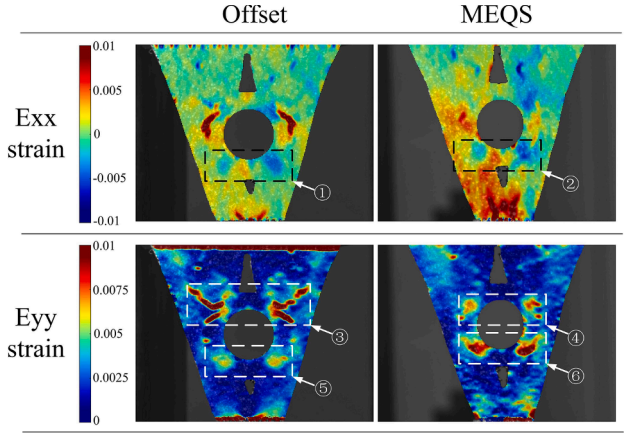

Fig. 15. DIC measured strain distributions in the Offset and MEQS samples.

In conclusion, the similarities observed in Figs. 15 and 16 demonstrate that the actual printing path-based finite element models reasonably well predicted the mechanical response of the composite structures in the elastic phase. Therefore, in the next session, the mechanical performance of the MEQS method was further numerically analysed using this actual printing path-based approach for another two composite structures.

4. Further case studies

4.1. Bridge case

The boundary condition of a bridge topology optimisation problem is illustrated in Fig. 17(a). A distributed load was applied on the upper rim along the direction of the black arrows. The 120 × 120 element-rectangular domain was optimised using the DCP method. The material property given in Table 1 was adopted in this case. The printing paths generated by the three concerned methods are illustrated in Fig. 17(b)-(d).

In this case, the reciprocal of the structural elastic strain energy is used as a measure of stiffness. The mechanical behaviours of the three models are given in Fig. 18. Similar to the results of the previous case, the stiffness corresponding to the printing paths generated by the EQS method is relatively worse. By comparing Fig. 17(b) and (c), it can be observed that the EQS method failed to achieve high-density filling of fibre reinforcements. According to the path design criteria summarised in Fig. 3, the MEQS method achieved a higher fibre reinforcement filling ratio in the local area of the structure compared to the Offset method, e.g. the red box area in Fig. 17(d).

As shown in Fig. 18, compared to the EQS method, the Offset method and the MEQS method have achieved improvement of 10.52 % and 37.65 %, respectively, in terms of structural stiffness. The maximum and minimum principal stress distribution is also given in Fig. 18. By comparing the minimum principal stresses, it can be seen that the stress distribution of the MEQS printing path is more uniform, and there are fewer occurrences of stress concentration compared to the Offset printing path. At the same time, the stress levels of almost all the printed continuous fibre filaments in the EQS model are much higher than the other two models, which may indicate that structures manufactured according to the EQS printing path may have lower strength in this case. Furthermore, by comparing the stress distribution within the black elliptical region in Fig. 18, it can be observed that due to the relatively higher fibre infill rate of the MEQS printing path in this area, the distribution of minimum principal stress was benefitted compared to the Offset printing path, which once again validates its effectiveness.

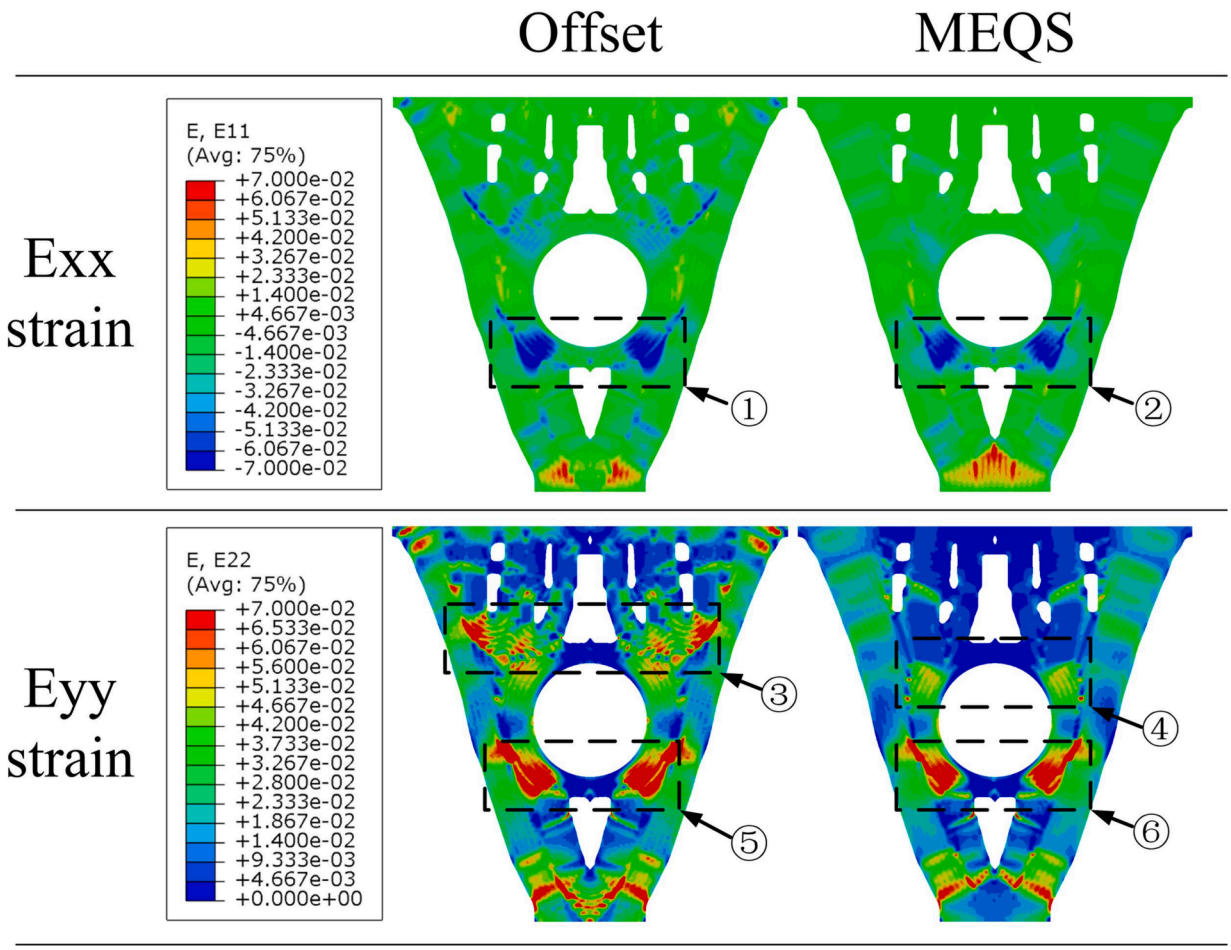

Fig. 16. FEA predicted strain distributions in the Offset and MEQS-based models.

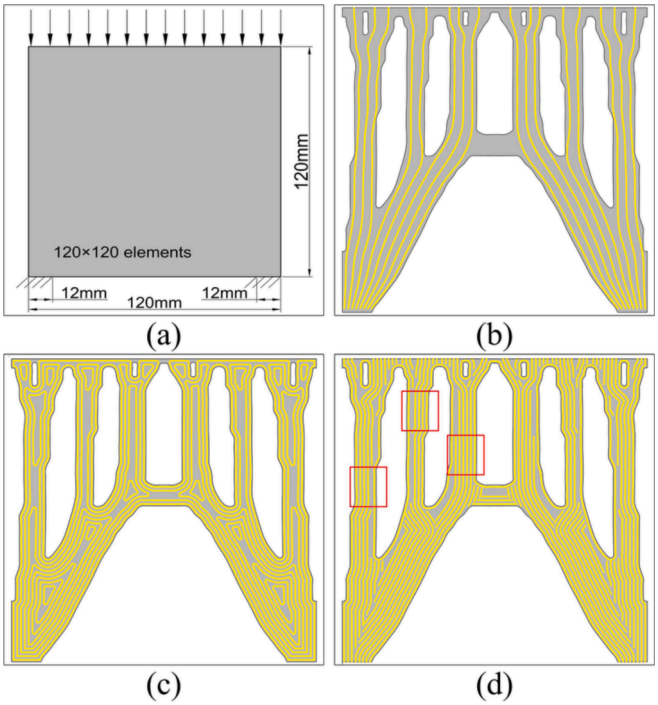

Fig. 17. (a) Boundary condition of the bridge case, and printing paths generated by: (b) EQS method, (c) Offset method and (d) MEQS method.

The comparison of von Mises stress of matrix material is given in Fig. 19. It can be seen that due to the inability of the EQS method to generate printing paths orthogonal to the main direction of the structure, the central part of the structure was complete lack of fibre reinforcement, resulting in relatively higher stress values.

4.2. *Messerschmitt-Bölkow-Blohm (MBB) case*

The boundary condition of an MBB beam is illustrated in Fig. 20(a). A concentrated load was applied along the direction of the black arrow. The 180 × 60 element-rectangular domain was optimised using the DCP method. The material property given in Table 1 was also adopted in this case. The printing paths generated by different methods are illustrated in Fig. 20(b)-(d). From Fig. 20(b), it can be observed that when planning the printing paths for the MBB beam using the EQS method, in order to avoid filament stacking at both ends of the MBB beam, only seven printing paths could be arranged within the MBB beam. These seven filaments were densely packed at the ends of the structure (as shown in the red box in Fig. 20(b)). In contrast, the central load-bearing portion of the MBB beam has a relatively larger width, but the total number of continuous fibre filaments in the structure remains the same, resulting in rather insufficient fibre reinforcement at the load-bearing position. Unlike the EQS method, both the Offset method and the MEQS method achieved much denser arrangement of printing paths at various local locations of the structure, consequently leading to better mechanical performance.

In this case, the reciprocal of the structural elastic strain energy was used as a measure of stiffness. The mechanical behaviours of the three models are given in Fig. 21. As shown in Fig. 21, compared to the EQS

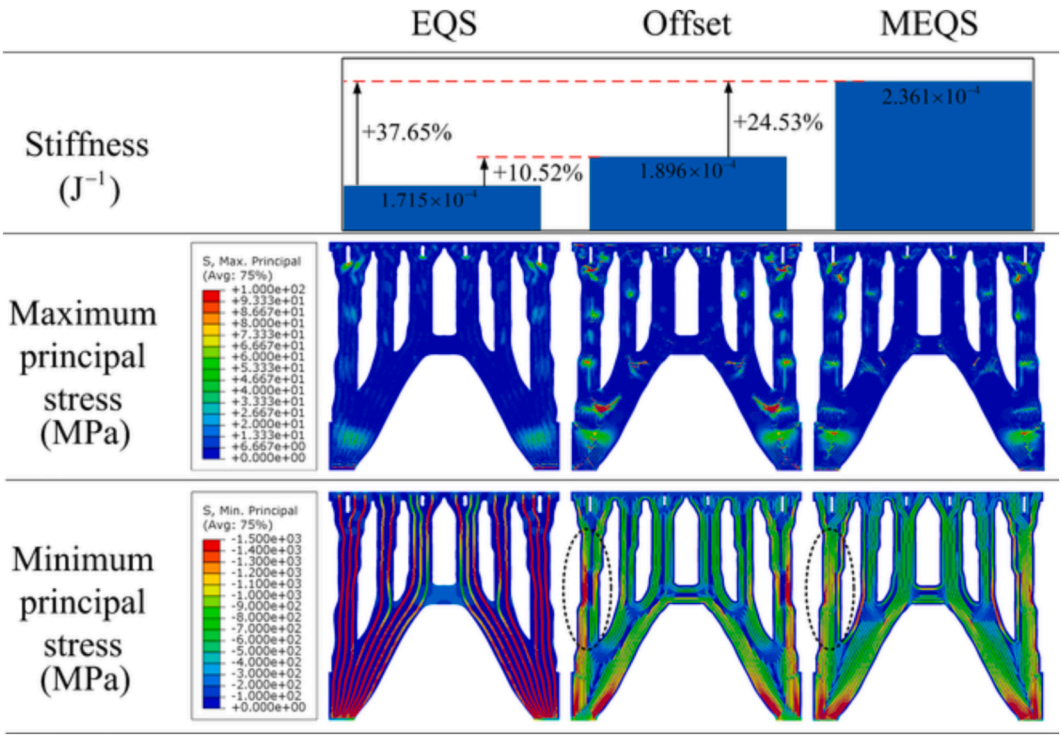

Fig. 18. Comparison of mechanical behaviours of the bridge case.

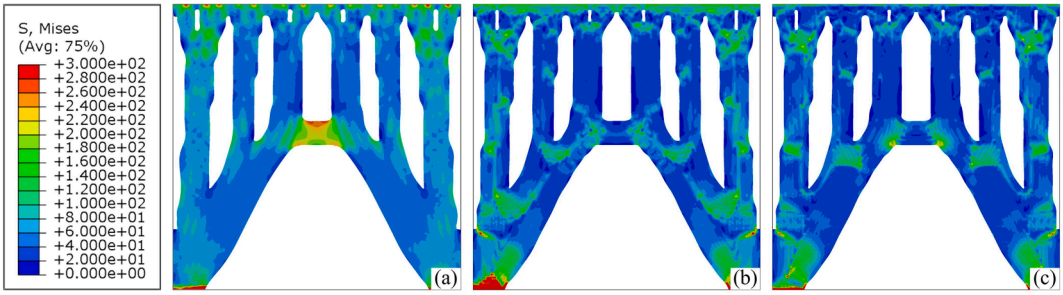

Fig. 19. Von Mises stress distributions in different models: (a) EQS, (b) Offset and (c) MEQS.

method, the Offset method and the MEQS method have achieved improvement of 85.81 % and 95.77 %, respectively, in terms of structural stiffness. Unlike previous cases, in this MBB beam case, the MEQS method did not show a significant performance improvement compared to the Offset method.

The principal stress distribution of the models is also given in Fig. 21, in which the stress distribution of the Offset model is very similar to that of the MEQS model. However, in the EQS model, the stress distribution of the filaments is similar to the EQS model in Fig. 18, with almost every filament experiencing higher stress. The phenomenon suggests that under the same load, the strength of the EQS model may be lower.

The distribution of von Mises stress was studied and given in Fig. 22. It can be observed that in certain areas around the internal voids of the MBB beam (highlighted by the black boxes), the von Mises stress concentration of the Offset and MEQS model is relatively insignificant, which can be concluded that both the Offset model and the MEQS model have a lower probability of matrix material failure under the same load compared to the EQS model.

5. Conclusions

This study presents a path planning method for additive manufacturing of continuous fibre composites based on structural geometric information, and combines it with the Discrete-Continuous Parameterization (DCP) topology optimisation method to construct a sequential topology optimisation-path planning framework. The method proposed in this research, called the modified equally-spaced (MEQS) method, improves upon the EQS method while incorporating the useful characteristics of the Offset method. The MEQS method generates loop-like printing paths around the internal voids of the structure for boundary reinforcement, creates continuous printing paths along the structure's boundaries to connect loading and constraint locations, as well as infills more fibres in locations without EQS fibre paths. Compared to the traditional EQS method, this modified method significantly increases the fibre infill rate and improves the structural performance. In this study, finite element analysis was conducted on an open-hole composite plate with complex geometric features after topology optimisation. The results show that the stiffness of the MEQS printing path was increased by 60.62 % compared to the EQS method, while the Offset method achieved only a 28.17 % stiffness improvement at a similar fibre infill rate.

Furthermore, experimental tests were performed on samples prepared with Offset and MEQS printing paths. The experimental results demonstrated a 15.52 % increase in stiffness and a 27.38 % increase in

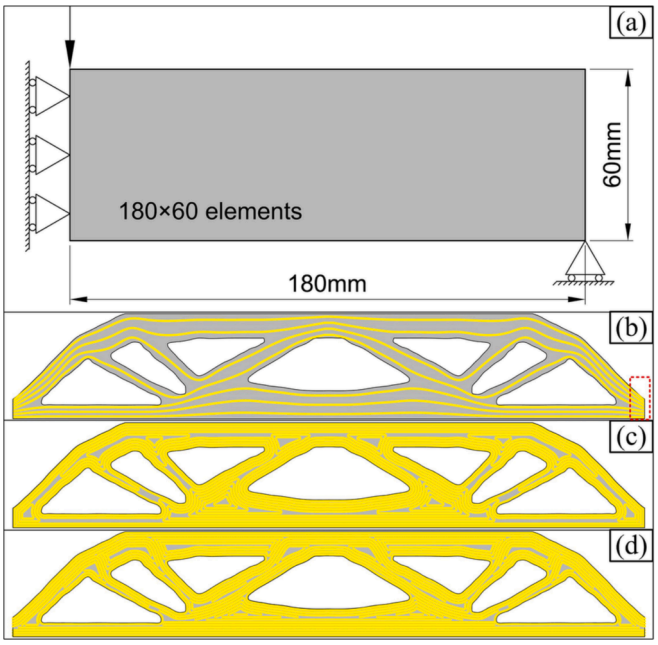

Fig. 20. (a) Boundary condition of the MBB beam and printing paths generated by: (b) the EQS method, (c) the Offset method and (d) the MEQS method.

strength for the MEQS printing path compared to the Offset printing path. The MEQS method was further validated through finite element modelling of a bridge case and an MBB case, both showing significant improvement in mechanical performance compared to the EQS printing path. However, in the MBB case with a relatively simple geometry under bending, the MEQS printing path did not exhibit a clear advantage over the Offset printing path, which to some extent indicated that the MEQS method may be more suitable for dealing with complex composite structures subjected to tension or compression. Further investigation is still needed to extend the MEQS to three-dimensional composite structures for more comprehensive evaluations under various loading conditions including multiaxial loads.

Although the MEQS method provides certain improvements in terms of stiffness and strength compared to methods such as Offset, there are still practical application issues to be overcome in future research: (1) Due to the possibility of circular paths in the MEQS printing path, when a 3D printer without a cutting mechanism is used for manufacturing, it is necessary to manually break and reconnect the circular paths to form a continuous printing path, which introduces human factors; (2) During the process of connecting the printing paths, some fine printing paths in the structure may be discarded, resulting in localised resin rich in the structure.

CRediT authorship contribution statement

Shuai Wang: Writing – original draft, Software, Methodology, Investigation, Conceptualization. **Haoqi Zhang:** Writing – original draft, Software, Methodology, Investigation. **Aonan Li:** Software, Data curation. **Junaid Ahmad Abdul Qayyum:** Data curation. **Yongxing Wang:** Methodology, Investigation. **Zhelong He:** Writing – review & editing, Supervision, Methodology. **Jie Liu:** Writing – review & editing, Supervision, Conceptualization. **Dongmin Yang:** Writing – review & editing, Supervision, Conceptualization.

Declaration of competing interest

The authors declare that they have no known competing financial

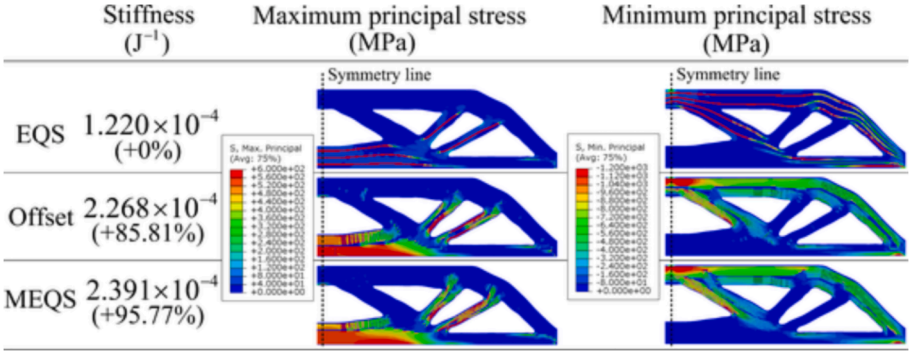

Fig. 21. Comparison of mechanical behaviours of the MBB beam.

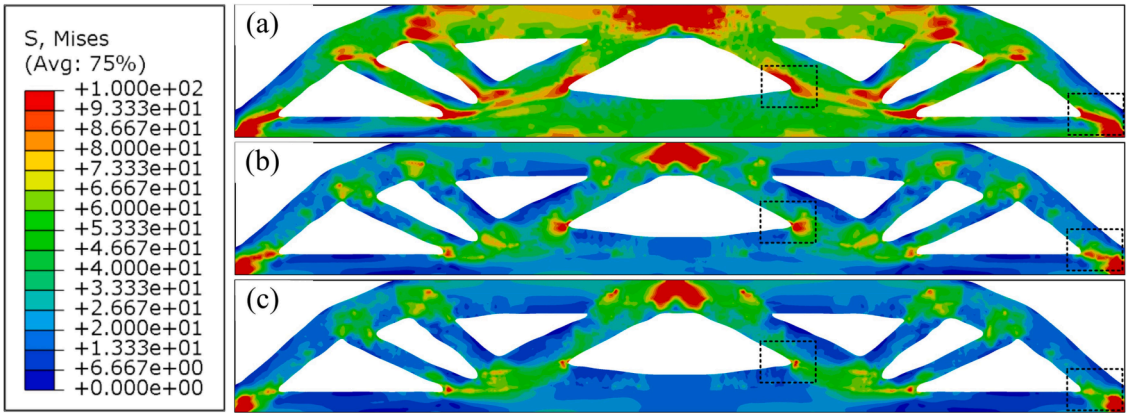

Fig. 22. Von Mises stress distribution in different models: (a) EQS, (b) Offset and (c) MEQS.

interests or personal relationships that could have appeared to influence the work reported in this paper.

Data availability

Data will be made available on request.

Acknowledgements

The authors would like to acknowledge Royal Society (IEC/NSFC/170418), National Science Foundation of China (Grant No. 51975199) and Natural Science Foundation of Hunan Province (Grant No. 2022JJ30004) for financial support of this study. Shuai Wang would like to acknowledge the support from China Scholarship Council (Grant No. 202006130128).

References

[1] Chawla KK. Composite materials: science and engineering. Springer Science & Business Media; 2012.
[2] Soutis C. Fibre reinforced composites in aircraft construction. Prog Aerosp Sci 2005;41(2):143–51.
[3] M.P. Bendsoe, N. Kikuchi, Generating optimal topologies in structural design using a homogenisation method, (1988).
[4] Sigmund O. A 99 line topology optimisation code written in Matlab. Struct Multidiscip Optimis 2001;21(2):120–7.
[5] Bendsoe MP, Sigmund O. Topology optimisation: theory, methods, and applications. Springer Science & Business Media; 2003.
[6] Wang MY, Wang X, Guo D. A level set method for structural topology optimisation. Comput Methods Appl Mech Eng 2003;192(1–2):227–46.
[7] Challis VJ. A discrete level-set topology optimisation code written in Matlab. Struct Multidiscip Optimis 2010;41(3):453–64.
[8] Chu DN, Xie Y, Hira A, Steven G. Evolutionary structural optimisation for problems with stiffness constraints. Finite Elem Anal Des 1996;21(4):239–51.
[9] Huang X, Xie M. Evolutionary topology optimisation of continuum structures: methods and applications. John Wiley & Sons; 2010.
[10] Guo X, Zhang W, Zhong W. Doing topology optimisation explicitly and geometrically—a new moving morphable components based framework. J Appl Mech 2014;81(8).
[11] Norato J, Bell B, Tortorelli DA. A geometry projection method for continuum-based topology optimisation with discrete elements. Comput Methods Appl Mech Eng 2015;293:306–27.
[12] Hoang V-N, Nguyen N-L, Nguyen-Xuan H. Topology optimisation of coated structure using moving morphable sandwich bars. Struct Multidiscip Optim 2020;61(2):491–506.
[13] Davim JP, Reis P. Drilling carbon fiber reinforced plastics manufactured by autoclave—experimental and statistical study. Mater Des 2003;24(5):315–24.
[14] Karataş MA, Gökkaya H. A review on machinability of carbon fiber reinforced polymer (CFRP) and glass fiber reinforced polymer (GFRP) composite materials. Defence Technol 2018;14(4):318–26.
[15] Zhang H, Dickson AN, Sheng Y, McGrail T, Dowling DP, Wang C, et al. Failure analysis of 3D printed woven composite plates with holes under tensile and shear loading. Compos B Eng 2020;186:107835.
[16] Li N, Link G, Wang T, Ramopoulos V, Neumaier D, Hofele J, et al. Path-designed 3D printing for topological optimised continuous carbon fibre reinforced composite structures. Compos B Eng 2020;182:107612.
[17] Stegmann J, Lund E. Discrete material optimisation of general composite shell structures. Int J Numer Meth Eng 2005;62(14):2009–27.
[18] Jiang D, Hoglund R, Smith DE. Continuous fiber angle topology optimisation for polymer composite deposition additive manufacturing applications. Fibers 2019;7(2):14.
[19] Luo Y, Chen W, Liu S, Li Q, Ma Y. A discrete-continuous parameterisation (DCP) for concurrent optimisation of structural topologies and continuous material orientations. Compos Struct 2020;236:111900.
[20] Elvas A, Sohouli A, Suleman A. Simultaneous topology and fiber path optimisation of composite structures with MAC constraints. Compos Struct 2022;294:115645.
[21] Yan X, Xu Q, Huang D, Zhong Y, Huang X. Concurrent topology design of structures and materials with optimal material orientation. Compos Struct 2019;220:473–80.
[22] Jantos DR, Hackl K, Junker P. Topology optimisation with anisotropic materials, including a filter to smooth fiber pathways. Struct Multidiscip Optim 2020:1–20.
[23] Zhang H, Wang S, Zhang K, Wu J, Li A, Liu J, et al. 3D printing of continuous carbon fibre reinforced polymer composites with optimised structural topology and fibre orientation. Compos Struct 2023;313:116914.
[24] Wang T, Li N, Link G, Jelonnek J, Fleischer J, Dittus J, et al. Load-dependent path planning method for 3D printing of continuous fiber reinforced plastics. Compos A Appl Sci Manuf 2021;140:106181.
[25] Papapetrou VS, Patel C, Tamijani AY. Stiffness-based optimisation framework for the topology and fiber paths of continuous fiber composites. Compos B Eng 2020;183:107681.
[26] Fernandes RR, van de Werken N, Koirala P, Yap T, Tamijani AY, Tehrani M. Experimental investigation of additively manufactured continuous fiber reinforced composite parts with optimised topology and fiber paths. Addit Manuf 2021;44:102056.
[27] Lin H, Brown LP, Long AC. Modelling and simulating textile structures using TexGen, Advanced Materials Research. Trans Tech Publ; 2011. p. 44–7.
[28] Nomura T, Dede EM, Lee J, Yamasaki S, Matsumori T, Kawamoto A, et al. General topology optimisation method with continuous and discrete orientation design using isoparametric projection. Int J Numer Meth Eng 2015;101(8):571–605.
[29] Liu J. Piecewise length scale control for topology optimisation with an irregular design domain. Comput Methods Appl Mech Eng 2019;351:744–65.
[30] Chen Y, Ye L. Topological design for 3D-printing of carbon fibre reinforced composite structural parts. Compos Sci Technol 2021;204:108644.
[31] Huang Y, Tian X, Zheng Z, Li D, Malakhov AV, Polilov AN. Multiscale concurrent design and 3D printing of continuous fiber reinforced thermoplastic composites with optimised fiber trajectory and topological structure. Compos Struct 2022;285:115241.
[32] Zhang H, Wu J, Robert C, Brádaigh CMÓ, Yang D. 3D printing and epoxy-infusion treatment of curved continuous carbon fibre reinforced dual-polymer composites. Compos B Eng 2022;234:109687.
[33] Blaber J, Adair B, Antoniou A. Ncorr: open-source 2D digital image correlation matlab software. Exp Mech 2015;55(6):1105–22.